

Progressive Frame Patching for FoV-based Point Cloud Video Streaming

Tongyu Zong, Yixiang Mao, Chen Li, Yong Liu, *Fellow, IEEE*, and Yao Wang, *Fellow, IEEE*

Abstract—Many XR applications require the delivery of volumetric video to users with six degrees of freedom (6-DoF) movements. Point Cloud has become a popular volumetric video format. A dense point cloud consumes much higher bandwidth than a 2D/360 degree video frame. User Field of View (FoV) is more dynamic with 6-DoF movement than 3-DoF movement. To save bandwidth, FoV-adaptive streaming predicts a user's FoV and only downloads point cloud data falling in the predicted FoV. However, it is vulnerable to FoV prediction errors, which can be significant when a long buffer is utilized for smoothed streaming. In this work, we propose a multi-round progressive refinement framework for point cloud video streaming. Instead of sequentially downloading point cloud frames, our solution simultaneously downloads/patches multiple frames falling into a sliding time-window, leveraging the inherent scalability of octree-based point-cloud coding. The optimal rate allocation among all tiles of active frames are solved analytically using the heterogeneous tile rate-quality functions calibrated by the predicted user FoV. Multi-frame downloading/patching simultaneously takes advantage of the streaming smoothness resulting from long buffer and the FoV prediction accuracy at short buffer length. We evaluate our streaming solution using simulations driven by real point cloud videos, real bandwidth traces, and 6-DoF FoV traces of real users. Our solution is robust against the bandwidth/FoV prediction errors, and can deliver high and smooth user quality in the face of bandwidth variations and dynamic user and point cloud movements.

Index Terms—Volumetric video streaming, Point cloud, Progressive downloading, Rate allocation, KKT condition.

I. INTRODUCTION

Point cloud video streaming will take telepresence to the next level by delivering full-fledged 3D information of the remote scene and facilitating six-degree-of-freedom (6-DoF) viewpoint selection to create a truly immersive experience. Leaping from planar (2D) to volumetric (3D) video poses significant communication and computation challenges. A point cloud video consists of a sequence of frames that characterize the motions of one or multiple physical/virtual objects. Each frame is a 3D snapshot, in the form of point cloud captured by a 3D scanner, e.g., LiDAR camera, or a camera array using photogrammetry. A high-fidelity point cloud frame of a single object can easily contain one million points, each of which has three 32-bit Cartesian coordinates and three 8-bit color attributes. At 30 frames/second, the raw data rate of a point cloud video (PCV) of a single object reaches 3.6 Gbps. The raw data rate required to describe a 3D scene with multiple objects increases proportionally.

T. Zong, Y. Mao, C. Li, Y. Liu and Y. Wang are with the Department of Electrical and Computer Engineering, New York University, Brooklyn, NY, 11201 USA e-mail: ({tz1178,yixiang.mao,chen.lee,yongliu,yw523}@nyu.edu).

Meanwhile, on the receiver side, a PCV viewer enjoys 6-DoF viewpoint selection through translational (x, y, z) and head rotational (*pitch, yaw, roll*) movements. Given the relative position between the object and the viewer's viewpoint, the compressed PCV will be decompressed and rendered on a 2D or 3D display, which also consumes significant computation resources. Furthermore, to facilitate seamless interaction and avoid motion sickness, the rendered view has to be delivered with short latency (e.g. <20 ms) after the viewer movement, the so called Motion-to-Photon (MTP) latency constraint [1]. As a result, PCV not only consumes more bandwidth and computation resources, it is additionally subject to stringent end-to-end latency budget for processing and delivery.

The goal of this work is to address the high-bandwidth, high-complexity and low-latency challenges of point cloud video by designing a novel progressive refinement streaming framework, where multiple frames falling into a sliding time window are patched simultaneously for multiple rounds, leveraging the inherent scalability of octree-based point-cloud coding. We will focus on video-on-demand applications, leaving the live PCV streaming and the ultimate challenge of realtime two-way interactive PCV streaming for future research.

Towards developing this progressive streaming framework, we made the following contributions:

- 1) We design a novel *sliding-window based progressive streaming framework* to gradually refine the spatial resolution of each tile as its playback time approaches and the FoV prediction accuracy improves. We investigate the trade-off between the need of long-buffer for absorbing bandwidth variations and the need of short-buffer for accurate FoV prediction.
- 2) We propose a novel point cloud tile rate-quality model that reflects the Quality of Experience (QoE) of PCV viewers both theoretically and empirically.
- 3) The tile rate allocation decision is formulated as a utility maximization problem. To get the optimal solution, an analytical algorithm based on Karush–Kuhn–Tucker (KKT) conditions is developed.
- 4) The superiority of our proposed algorithm is evaluated using PCV streaming simulations driven by real point cloud video codec and real-world bandwidth traces.

II. RELATED WORK

Impressive research have been accomplished for coding [2]–[6], streaming [7]–[22], FoV prediction [23]–[27], and edge-assisted delivery [28]–[31] of 360° video in recent years. However, a 360° video only covers the whole viewing sphere

captured from a center position, records 2D projection along each direction from the center, and is typically projected onto a 2D plane and processed as a planar video. A viewer mostly makes 3-DoF head rotational movements, rotate her head in 2-DoF (pitch and yaw). A PCV records the 3D space directly and allows 6-DoF viewpoint selection from different positions and angles.

Several PCV coding and streaming systems, e.g. [32]–[58], have shown promises. For example, [32] proposes patchVVC, a point cloud patch-based compression framework that is FoV adaptive, and achieves both high compression ratio and real-time decoding. The authors of YOGA [33] propose a frequency-domain-based profiling method to transform point cloud into a vector before estimating the compressed bitrate for geometry data and color information using linear regression. Then they perform rate allocation between geometry map and attribute map in the context of V-PCC [59]. The Hermes system [35] adopts an implicit correlation encoder to reduce bandwidth consumption and proposes a hybrid streaming method that adapts to dynamic viewports. The ViVo system [37] adopts frame-wise k-d tree representation using DRACO [60], which is simple but less efficient than the recently established MPEG G-PCC standard [59]. It uses tile-based coding to enable FoV adaptation and employs non-scalable multiple-rate versions of the same tile for rate adaptation. Moreover, it only performs prefetching over a short interval ahead, leading to limited robustness to network dynamics. Another study [39] considered delivering low-resolution PCV and used deep-learning models to enhance the resolution on the receiver, which enhances coding efficiency but does not facilitate FoV adaptation. [61] extends the concept of dynamic adaptive streaming over HTTP (DASH) towards DASH-PC (DASH-Point Cloud) to achieve bandwidth and view adaptation for PCV streaming. It proposes a clustering-based sub-sampling approach for adaptive rate allocation, while our work is able to optimize the rate allocation explicitly based on the FoV prediction accuracy and tile utility function. [47] presents a generic and real-time time-varying point cloud encoder, which not only adopts progressive intra-frame encoding, but also encodes inter-frame dependencies based on an inter-prediction algorithm. To better match user's FoV, the authors of [55] propose a hybrid visual saliency and hierarchical clustering based tiling scheme. They also propose a joint computational and communication resource allocation scheme to optimize the QoE. Most of the existing studies focused on streaming PCV of a single object without *explicit* rate control. In this work, we assume octree-based scalable PCV coding which simultaneously enables spatial scalability and FoV adaptation with fine granularity. Our proposed progressive streaming framework takes full advantage of scalable PCV coding to enhance streaming robustness.

[36] is the first work to propose a window-based streaming buffer that supports rate update for all tiles in the buffer and the tile rate allocation problem is solved by a heuristic greedy algorithm. Furthermore, it proposes a tile utility function to model the true user QoE. However, it is not clear how the coefficients of the utility model are obtained. We formulate the PCV streaming problem with the well developed concept

of scalable octree coding, and propose a more refined utility model that better reflects viewer's visual experience when viewing a point cloud tile from certain distance. To achieve this, we coded several test PCVs using MPEG G-PCC and found that the level of detail (LoD) is logarithmically related to the rate. Due to tile diversity, the data rate needed to code octree nodes up to a certain level is highly tile-dependent. We fit the coefficients of this logarithmic mapping from rate to LoD and model the tile utility as a function of angular resolution to match the shape of subjective utility-(rate, distance) curve in [37]. We also develop a new tile rate allocation algorithm based on the KKT Condition that outperforms the heuristic algorithm of [36] in our evaluation.

III. FOV-ADAPTIVE CODING AND STREAMING

A. Octree-based Scalable PCV Coding

MPEG has considered point cloud coding (PCC) and recommended two different approaches [59]. The V-PCC approach projects a point cloud frame into multiple planes and assembles the projected planes into a single 2D frame, and code the resulting sequence of frames using previously established video coding standard HEVC. The G-PCC approach represents the geometry of all the points using an octree, and losslessly represents the octree using context-based entropy coding. The color attributes are coded following the octree structure as well using a wavelet-like transform. By leveraging the efficiency of HEVC, especially in exploiting temporal redundancy through motion compensated prediction, the V-PCC approach is more mature and is currently more efficient than the G-PCC for dense point clouds. However, V-PCC does not allow selective transmission of regions intersecting with the viewer's FoV or objects of interests. It is also not efficient for sparse clouds such as those captured by LiDAR sensors. The spatial scalability can be indirectly enabled by coding the projected 2D video using spatial scalability, but this does not directly control the distance between the points and cannot be done at the region level.

A point cloud can be coded using an octree which is recursively constructed: the root node represents the entire space spanned by all the points, which is equally partitioned along the three dimensions into $2 \times 2 \times 2$ cubes; the root has eight children, each of which is the root of a sub-octree representing each of the eight cubes. The recursion stops at either an empty cube, or the maximum octree level L . Each sub-octree rooted at level l represents a cube with side lengths that are $1/2^l$ of the side lengths of the original space. To code the geometry, the root node records the (x, y, z) coordinates of the center of the space, based on which the coordinates of the center of any cube at any level are uniquely determined. Consequently, each non-root node only needs one bit to indicate whether the corresponding cube is empty or not. For the octree in Fig. 1b, the nodes with value 1 at the three levels represent one, two and three non-empty cubes with side lengths of $1/2$, $1/4$ and $1/8$ in Fig. 1a, respectively. All the non-empty nodes at level l collectively represent the geometry information of the point cloud at the spatial granularity of $1/2^l$. This makes octree *spatially scalable*: with one more

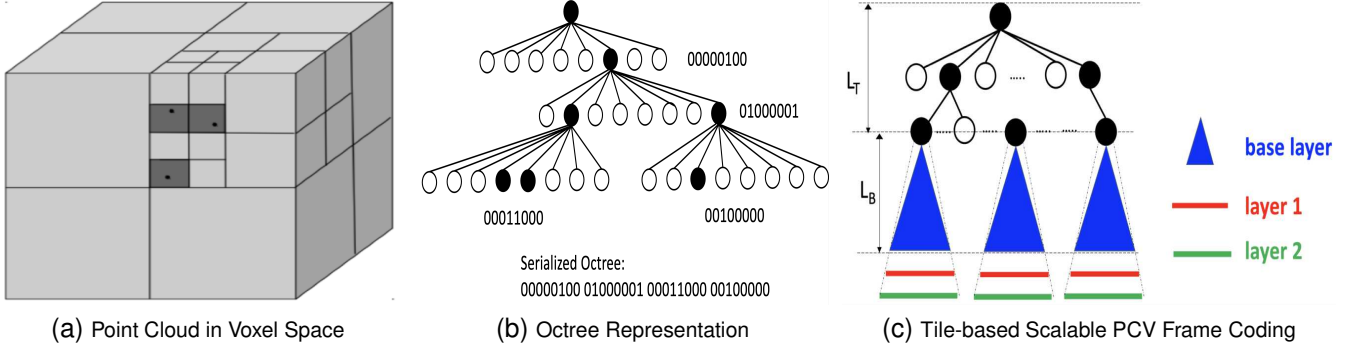


Fig. 1: Octree-based Scalable and FoV-adaptive Point Cloud Coding

level of nodes delivered, the spatial resolution doubles (i.e., the distance between points is halved). The color attributes of a point cloud are coded following the octree structure as well, with each node stores the average color attributes of all the points in the corresponding cube. Scalable color coding can be achieved by only coding the difference between a node and its parent. The serialized octree can be further losslessly compressed using entropy coding. With MPEG G-PCC, at each tree level l , the status of a node (0 or 1) is coded using context-based arithmetic coding, which uses a context consisting of its neighboring siblings that have been coded and its neighboring parent nodes to estimate the probability p that the node is 1.

B. Tile-based Coding and Streaming

Considering the limited viewer Field-of-View (FoV) (dependent on the 6-DoF viewpoint), occlusions between objects and parts of the same object, and the reduced human visual sensitivity at long distances, only a subset of points of a PCV frame are *visible and discernible* to the viewer at any given time. FoV-adaptive PCV streaming significantly reduces PCV bandwidth consumption by only streaming points visible to the viewer at the spatial granularity that is discernible at the current viewing distance. To support FoV-adaptive streaming, octree nodes are partitioned into slices that are selectively transmitted for **FoV adaptability** and **spatial scalability**. Each slice consists of a subset of nodes at one tree level that are independently decodable provided that the slice containing their parents is received. Without considering FoV adaptability, one can simply put all nodes in each tree level into a slice to achieve spatial scalability. The sender will send slices from the top level to the lowest level allowed by the rate budget. To enable FoV adaptability, a popular approach known as tile-based coding is to partition the entire space into non-overlapping 3D tiles and code each tile independently using a separate tile octree. Only tiles falling into the predicted FoV will be transmitted. To enable spatial scalability within a tile, we need to put the nodes at each level of the tile octree into a separate slice. As illustrated in Fig. 1c, each sub-octree rooted at level L_T represents a 3D-tile with side length of $1/2^{L_T}$. Within each tile sub-octree, nodes down to the L_B level are

packaged into a base layer slice, and nodes at the lower layers are packaged into additional enhancement layer slices.

When the streaming server is close to the viewer, one can conduct reactive FoV-adaptive streaming: the client collects and uploads the viewer's FoV to the server; the server renders the view within the FoV, and streams the rendered view as a 2D video to the viewer. To facilitate seamless interaction and avoid motion sickness, the rendered view has to be delivered with short latency (e.g. <20 ms) after the viewer movement, the so called Motion-to-Photon (MTP) latency constraint [1]. To address the MTP challenge, we consider predictive streaming that predicts the viewer's FoVs for future frames and prefetches tiles within the predicted FoV [36]–[38].

IV. PROGRESSIVE PCV STREAMING

Due to the close interaction with PCV objects, viewers are highly sensitive to QoE impairments, such as black screen, freezes, restarts, excessively long latency, etc. Not only the network and viewer dynamics have direct QoE impacts, bandwidth and FoV prediction errors are also critical for the effectiveness of predictive streaming. We propose a novel *progressive FoV-adaptive PCV streaming design* to minimize the occurrence of the above impairments and deliver a high level of viewer QoE.

A. Progressive Downloading/Patching

Most of the existing FoV-adaptive streaming solutions can be categorized as *Sequential-Decision-Making (SDM)*: at some time point τ before the playback deadline t of a frame, one predicts the viewer FoV at t , downloads tiles falling into the predicted FoV at video rates determined by some rate adaptation algorithm, then repeats the process for the next frame. $t - \tau$ is the time interval for both FoV prediction and frame pre-fetching, which is upper bounded by the client side video buffer length. To achieve smooth streaming, a long pre-fetching interval is preferred to absorb the negative impact of bandwidth variations. However, FoV prediction accuracy decays significantly at long prediction intervals. We have studied the optimal trade-off for setting the buffer length for on-demand streaming of 360° video in [15], [16].

Scalable PCV coding opens up a new dimension to reconcile the conflicting desires for long streaming buffer and short FoV

prediction interval. It allows us to **progressively download and patch** tiles: when a frame's playback deadline is still far ahead, we only have a rough FoV estimate for it, and will download low resolution slices of tiles overlapping with the predicted FoV; as the deadline approaches, we have more accurate FoV prediction, and will *patch* the frame by downloading additional enhancement slices, for tiles falling into the predicted FoV. *Progressive streaming is promising to simultaneously achieve streaming smoothness and robustness against bandwidth variations and FoV prediction errors.* On one hand, as shown in Fig. 2, each tile in each segment is downloaded over multiple rounds, the interval of which is Δ . A segment consists of S frames with the total video duration of Δ . Within each round, multiple segments are downloaded simultaneously. And the final rendered quality of each tile is a function of the total downloaded rate (thanks to the scalable coding, there is minimal information redundancy between the multiple progressive downloads). The final rendered quality is less vulnerable to network bandwidth variations and the FoV prediction errors at individual time instants. On the other hand, tile downloading and patching are guided by FoV predictions at multiple time instants with accuracy improving over time. If a tile falls into the predicted FoV in multiple rounds, the likelihood that it will fall into the actual FoV is high, and its quality will be *reinforced* by progressive downloading; if a tile only shows up once in the predicted FoV when its playback time is still far ahead, the chance for it to be in the actual FoV is small. Fortunately, the bandwidth wasted in downloading the low-resolution slices is low.

B. Optimal Rate Allocation

Progressive streaming conducts **Parallel-Decision-Making (PDM)**. For a tile k in the frame to be rendered at t , we prefetch it in the previous I rounds, from $t - I$ to $t - 1$. Let $r_i(t, k)$ denote its download rate in round $t - i$. The final rate for this tile is $\sum_{i=1}^I r_i(t, k)$. Meanwhile, at download time τ , all tiles of frames with playback time from $\tau + 1$ to $\tau + I$ are being downloaded/patched at rates $\{r_i(\tau + i, k), 1 \leq i \leq I, \forall k\}$, and the total rate is bounded by the available bandwidth $B(\tau)$, i.e.,

$$\sum_{i=1}^I \sum_k r_i(\tau + i, k) \leq B(\tau).$$

One greedy solution for bandwidth allocation at download time τ is to maximize the expected quality enhancements for all the active frames, based on the current FoV estimations:

$$\begin{aligned} \max_{\{r_i(\tau+i,k)\}} & \sum_{i=1}^I \sum_k w_i \tilde{p}_{\tau+i,k} \cdot \left\{ Q \left(\sum_{j=i}^I r_j(\tau + j, k), \tilde{d}_{\tau+i,k} \right) \right. \\ & \left. - Q \left(\sum_{j=i+1}^I r_j(\tau + j, k), \tilde{d}_{\tau+i,k} \right) \right\}, \end{aligned} \quad (1)$$

where $Q(r, d)$ reflects the rendered quality of a tile at rate r when viewed from distance d , $\tilde{p}_{\tau+i,k}$ and $\tilde{d}_{\tau+i,k}$ are the predicted view likelihood and view distance for tile k of frame to be rendered at time $\tau + i$, and w_i is a decreasing function of

i , considering that FoV estimate accuracy drops for far away frames.

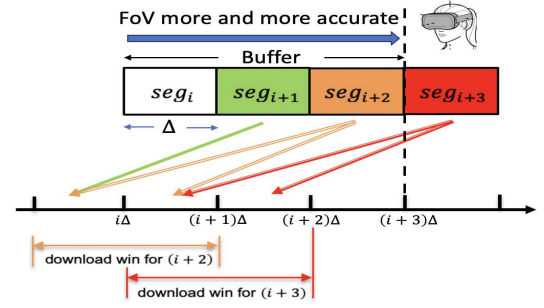


Fig. 2: Progressive Streaming Example with Sliding-window Size of 3: in round $i\Delta$, the base layer of all tiles within segment $i + 3$ within the predicted FoV for that segment are being downloaded for the first time, while frames within segment $i + 2$ are being patched with enhancement layers for tiles falling into the predicted FoV. Frames of segment $i + 3$ will be patched in the next round $(i + 1)\Delta$.

C. View-distance based Tile Utility Model

In this section, we explain in detail the proposed tile utility model $Q(r, d)$ in Equation (1). Tile quality depends on its angular resolution f_{ang} , which is the number of points per degree that are visible to the user within the tile. There are many subjective study about the quality of rendered images or videos, but most of them only consider the impact of rate, while very few consider the distance between the viewer and the object, which can be very dynamic in PCV streaming. A subjective study in [37] suggests that users' QoE changes significantly when they view a rendered point cloud object at different distances. The authors showed a reasonable curve telling the relations between utility, rate and viewing distance. Unfortunately, it didn't provide a specific utility model. In our work, we try to find a specific tile utility function with respect to viewing distance and tile rate that generates the same trend of curve in [37]. For the traditional 2D video frames/tiles, which is assumed to be viewed from a fixed distance, we can infer the direct mapping from rate to quality, which is usually a logarithm function. However, it is not that clear how the rate and viewing distance simultaneously impact the perceived quality of point cloud tiles. A quality model of image with respect to both distance and resolution was proposed in [62], but it doesn't directly fit with point cloud video. Nevertheless, it is inspired from [62] that the perceived quality for an object depends on the angular resolution, which depends on the viewing distance and physical size of the object, as well as image resolution. Following [62], we assume that the perceived quality of a viewed tile is logarithmically increasing with the angular resolution f_{ang} , which is the number of points per degree within the tile. With more and more points inside the tile, the per-degree utility increases but more and more slowly. Let $\log(c \cdot f_{ang})$ be the per-degree quality of a tile, we assume that the perceived quality of a tile

that covers θ degree in either horizontal or vertical direction is

$$Q(f_{ang}, \theta) = \theta \cdot \log(c \cdot f_{ang}),$$

where c is a constant factor to be determined by the saturation threshold. As shown in Fig. 3, each tile is a subtree, and f_{ang} is decided by the level of detail (LoD) which is the subtree's height H within the tile, and the viewer's span-in-degree θ across the tile:

$$f_{ang} = \frac{2^H}{\theta} = \frac{d \cdot 2^H \cdot \pi}{wid \cdot 180},$$

where d is the distance between the viewer and the tile, and wid is the physical side length of a tile. Therefore, the tile utility model is:

$$Q(H, d) = \frac{M}{d} \cdot \log(c \cdot \frac{d \cdot 2^H}{M}), \quad (2)$$

where $M = wid \cdot 180/\pi$.

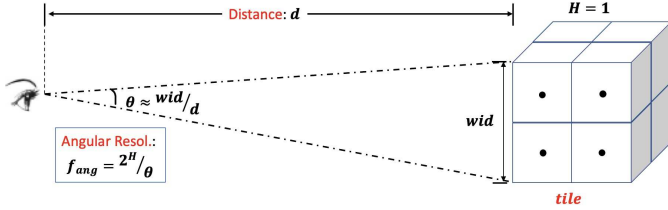


Fig. 3: Tile Angular Resolution dependent on distance between the user and the tile as well as subtree's height within the tile.

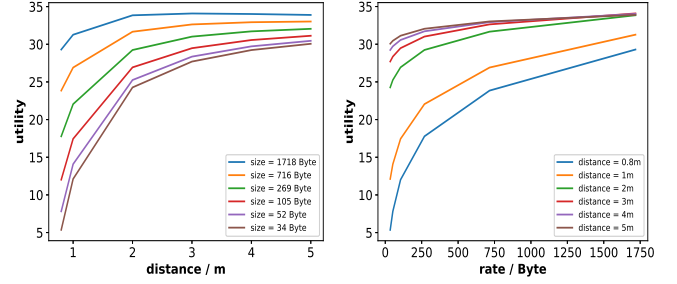
To achieve a level of detail (LoD) H , all nodes up to level H of the tile subtree has to be delivered, which will incur a certain rate (the total number of bits to code a tile to level H). We have coded several test PCVs using MPEG G-PCC and found that the LoD is logarithmically related to the rate. Due to tile diversity, the data rate needed to code octree nodes up to level H is highly tile-dependent. In other words, given a coding rate budget r , the achievable LoD is tile-dependent. Let $H_{i,k}(r)$ be the rate-LoD mapping for tile k within frame i , we assume

$$H_{i,k}(r) = a_{i,k} \log(b_{i,k} r + 1),$$

where the parameters $a_{i,k}, b_{i,k}$ are obtained by fitting the actual rate data for the tiles coded using G-PCC. Substituting this expression into (2) yields:

$$Q_{i,k}(r, d) = \frac{M}{d} \cdot \left(a_{i,k} \log 2 \cdot \log(b_{i,k} \cdot r + 1) + \log\left(\frac{c \cdot d}{M}\right) \right). \quad (3)$$

Note that tile utility is not necessarily 0 at $r = 0$, because there is possibly one point inside the tile. There's only one parameter to be decided: c , which controls the shape of the curve. We decide its value by reasoning that the utility should saturate at some point even if we keep increasing rate and/or distance. This is due to human visual acuity: generally we cannot resolve any two points denser than 60 points per degree [63]. In other words, the derivative of $Q_{i,k}$ with respect to d should



(a) Utility-Distance curve at different tile rates. (b) Utility-Rate curve at different distances.

Fig. 4: Tile Utility Curve.

be zero given any rate when d is so large that the angular resolution f_{ang} reaches 60° :

$$\frac{\partial Q}{\partial d} = \frac{M}{d^2} (1 - \log(c \cdot f_{ang}))$$

The derivative goes to zero when f_{ang} is 60° if $c = \frac{e}{60}$.

Then we can get the curve similar to the one in [37]. Taking a tile for example, the utility curve with respect to tile rate and distance is shown below. It's a tile from point cloud video *Long Dress* of 8i [44], where the figure is 1.8m high and tile is at the 4th level of the whole octree. For more details about the dataset, please refer to Section V. For simplicity, we ignore the subscripts of $Q_{i,k}$ as Q in the following sections.

D. Water-filling Rate Allocation Algorithm

We now develop an analytical algorithm for solving the utility maximization problem formulated in Sec. IV-B. In Equation (1), the second term $Q\left(\sum_{j=i+1}^I r_j(\tau + i, k), \tilde{d}_{\tau+i,k}\right)$ represents the tile quality of the layers that have been downloaded to the buffer before the current round, which is a given constant for the rate optimization at the current round. The utility maximization problem for each round is simplified as below, along with the constraints:

$$\max_{\{r_i(\tau+i,k)\}} \sum_{i=1}^I \sum_k w_i \tilde{p}_{\tau+i,k} \cdot Q\left(\sum_{j=i}^I r_j(\tau + i, k), \tilde{d}_{\tau+i,k}\right) \quad (4a)$$

subject to

$$r_i(\tau + i, k) \geq 0, \quad 1 \leq \tau \leq T + I - 1, 1 \leq i \leq I, \forall k, \quad (4b)$$

$$\sum_{j=i}^I r_j(\tau + i, k) \leq R(\tau + i, k), \quad 1 \leq \tau \leq T + I - 1, \quad 1 \leq i \leq I, \forall k, \quad (4c)$$

$$\sum_{i=1}^I \sum_k r_i(\tau + i, k) \leq B(\tau), \quad 1 \leq \tau \leq T + I - 1, \quad (4d)$$

where T is the video length, and $R(\tau + i, k)$ is the maximum rate of each tile $(\tau + i, k)$. The tile rate allocation problem is similar to the typical water-filling problem, where we "fill" the tiles in an optimal order based on their significance determined by the existing rates, probability to be viewed, distance from the viewer, and the calibration weights $\{w_i\}$.

Equation (4) is a nonlinear optimization problem so that the Karush–Kuhn–Tucker (KKT) conditions serve as the first-order necessary conditions. Furthermore, the KKT conditions for this problem are also sufficient due to the fact that the tile utility model $Q(r, d)$ is concave in terms of r with a given d , and the inequality constraints (4b) and (4c) are continuously differentiable and convex, and (4d) is an affine function. Therefore, we apply KKT conditions to optimally solve this tile rate allocation problem as shown in Algorithm 1. And the detailed KKT condition-based optimization is explained in Section IV-E.

Algorithm 1 KKT Condition based Tile Rate Allocation

Input: update window size I , point cloud video, video length T , user FoV trace, bandwidth trace, utility coefficients of all tiles.

- 1: **for** τ in $1:T + I - 1$ **do**
 - 2: Predict FoV for all the tiles in the update window,
 get viewing probability of tiles: $\tilde{p}_{\tau+i,k}, 1 \leq i \leq I, \forall k$
 get viewing distances from user viewpoint to tiles:
 $\tilde{d}_{\tau+i,k},$
 - 3: Call KKT-Condition based optimization (**Algorithm 2**);
 - 4: Allocate tile rates based on the results;
 - 5: Evaluate quality for frames being watched by user;
 - 6: **end for**
-

E. KKT Condition-based Optimization

In this section, we explain how to embed KKT condition-based optimization into Problem 4. We follow the standard procedures of KKT conditions.

1) *Standard Formulation:* First, we need to simplify the symbols in Problem (4). At each update time τ , we call this KKT optimization, so we eliminate τ to simplify the variables: $\sum_{j=i}^I r_j(\tau+i, k)$ is replaced by $r_{i,k}$, which is the resulting tile rate after this update round. Also, we simplify the constants $R(\tau+i, k)$ as $R_{i,k}$, $\tilde{p}_{\tau+i,k}$ as $\tilde{p}_{i,k}$, and $\tilde{d}_{\tau+i,k}$ as $\tilde{d}_{i,k}$, where $1 \leq i \leq I$ and k is tile index within each frame i . What's more, we define $r_{i,k}^0 = \sum_{j=i+1}^I r_j(\tau+i, k)$, the existing downloaded rate for tile $(\tau+i, k)$. Problem 4 can be simplified as below:

$$\max_{\{r_{i,k}\}} \sum_{i,k} w_i \tilde{p}_{i,k} \cdot Q(r_{i,k}, \tilde{d}_{i,k}) \quad (5a)$$

subject to

$$r_{i,k} \geq r_{i,k}^0, \quad 1 \leq i \leq I, \forall k, \quad (5b)$$

$$r_{i,k} \leq R_{i,k}, \quad \forall 1 \leq i \leq I, \forall k, \quad (5c)$$

$$\sum_{i,k} (r_{i,k} - r_{i,k}^0) \leq B, \quad \forall 1 \leq i \leq I, \forall k, \quad (5d)$$

Next, we define several functions for different parts of Problem (4). Let $f(\mathbf{r}) = \sum_{i,k} w_i \tilde{p}_{i,k} \cdot Q(r_{i,k}, \tilde{d}_{i,k})$, $\mathbf{g}^1(\mathbf{r}) = -\mathbf{r} + \mathbf{r}^0$, $\mathbf{g}^2(\mathbf{r}) = \mathbf{r} - \mathbf{R}$, and $h(\mathbf{r}) = \sum_{i,k} (r_{i,k} - r_{i,k}^0) - B$, where \mathbf{r} , \mathbf{r}^0 and \mathbf{R} are vectors of $r_{i,k}$, $r_{i,k}^0$ and $R_{i,k}$ respec-

tively. Then we rewrite the above equations once more into the standard form of KKT condition:

$$\min_{\mathbf{r}} -f(\mathbf{r}) \quad (6a)$$

subject to

$$\mathbf{g}^1(\mathbf{r}) \leq 0, \quad (6b)$$

$$\mathbf{g}^2(\mathbf{r}) \leq 0, \quad (6c)$$

$$h(\mathbf{r}) = 0, \quad (6d)$$

2) *Analytical Algorithm:* The solutions satisfying KKT conditions for this problem are also sufficient because $f(\cdot)$ is concave, both $\mathbf{g}^1(\cdot)$ and $\mathbf{g}^2(\cdot)$ are continuously differentiable and convex, and $h(\cdot)$ is affine. We follow the standard steps to solve it. With Lagrange multipliers, (6) is transformed as:

$$\max_{\mu^1, \mu^2, \lambda} \min_{\mathbf{r}} L(\mathbf{r}, \mu^1, \mu^2, \lambda) = -f(\mathbf{r}) \quad (7a)$$

$$+ \mu^1 \cdot \mathbf{g}^1(\mathbf{r}) + \mu^2 \cdot \mathbf{g}^2(\mathbf{r}) + \lambda h(\mathbf{r}). \quad (7b)$$

Then we derive the properties of the solution based on the following KKT conditions:

Stationarity:

$$\frac{\partial L}{\partial \mathbf{r}} = 0, \quad (8)$$

therefore,

$$r_k = \frac{z_k}{\lambda + \mu_k^2 - \mu_k^1} - \frac{1}{b_k},$$

where $z_k = a_k \theta_k \log 2$ is a constant when θ_k is given.

Dual feasibility:

$$\mu_k^i \geq 0, \quad i = \{1, 2\}, \quad (9)$$

Complementary slackness:

$$\mu^i \cdot \mathbf{g}^i(\mathbf{r}) = 0, \quad i = \{1, 2\}, \quad (10)$$

therefore,

$$\mu_k^1(-r_k + r_k^0) = 0$$

$$\mu_k^2(r_k - R_k) = 0$$

Therefore, the optimal rate allocation has three possible solutions according to conditions (8) and (10):

$$r_k^* = \begin{cases} r_k^0 & \text{if } \lambda \geq \frac{z_k}{r_k^0 + 1/b_k}; \\ R_k & \text{if } \lambda \leq \frac{z_k}{R_k + 1/b_k}; \\ \frac{z_k}{\lambda} - \frac{1}{b_k} & \text{if } \lambda = \frac{z_k}{r_k^* + 1/b_k}. \end{cases} \quad (11)$$

Once λ is decided, all r_k^* s are decided. Therefore, the goal is to find the optimal λ . The analytical water filling algorithm for finding λ^* is described in Algorithm 2.

V. EVALUATION

In this section, we demonstrate the superiority of the proposed approach over several baselines.

Algorithm 2 Analytical Water Filling Algorithm

Input: given θ_k and utility parameters a_k and b_k , each tile k keeps two values: $V_k^1 = \frac{z_k}{r_k^0 + 1/b_k}$ and $V_k^2 = \frac{z_k}{R_k + 1/b_k}$.

- 1: **for** λ in $[0 : \max\{V_k^1\}]$ **do**
- 2: compare λ to both V_k^1 and V_k^2 , $\forall k$,
 obtain resulted r_k based on Equation (11).
- 3: **if** $\sum_k (r_k - r_k^0) = B$ **then**
- 4: $\lambda^* = \lambda$,
- 5: $r_k^* = r_k$, $\forall k$,
- 6: **break**.
- 7: **end if**
- 8: **end for**

A. Setup

1) *Datasets:* We used point cloud videos from the 8i website [64], which includes 4 videos, each with 300 frames with frame rate of 30 fps. The user FoV trace is from [44] which involves 26 participants watching looped frames of the 8i videos on Unity game engine. The bandwidth trace is from NYU Metropolitan Mobile Bandwidth Trace [65], which includes 4G bandwidth traces collected in NYC when traveling on buses, subways, or ferry.

2) *FoV Prediction and Bandwidth Prediction:* FoV prediction method used in this work is linear regression, while other approaches like neural network based prediction model can also be used in our proposed framework. More specifically, we predict at most future $I = 600$ frames simultaneously using past $0.5 \cdot I$ frames, which is an empirical best history window size reported in [37]. The FoV span is 90° . The prediction accuracy results with different future prediction window sizes are reported in Section V-C1. We predict future bandwidth by harmonic mean.

B. Baselines

- 1) **Non-progressive Downloading:** This baseline is similar to the traditional video streaming in 2D video with one new segment downloaded to the end of the streaming buffer in each round. The rate allocation between frames within each new segment is optimized using a KKT algorithm similar to Algorithm 1 and 2, based on just one-time FoV prediction result.
- 2) **Progressive with Equal-allocation:** To demonstrate the effectiveness of KKT based optimization approach for progressive streaming, we evaluate a naive progressive streaming baseline where the available bandwidth is equally allocated over all active tiles falling into the predicted FoV at each round.
- 3) **Rate-Utility Maximization Algorithm (RUMA):** In the related state-of-the-art work [36], the authors proposed a tile utility model where the tile utility is simply the logarithm of the tile rate multiplied by the number of differentiable points. Based on this model, the authors further proposed a greedy heuristic tile rate allocation algorithm which we call RUMA for short. RUMA didn't explicitly introduce the concept of scalable PCV coding. In our work, we formulate the PCV streaming problem

with a well developed concept of scalable coding, and propose a more refined utility model that better reflect viewer's visual experience when viewing a point cloud tile from certain distance. To achieve this, we have coded several test PCVs using MPEG G-PCC and found that the level of detail (LoD) is logarithmically related to the rate. Due to tile diversity, the data rate needed to code octree nodes up to level H is highly tile-dependent. In other words, given a coding rate budget r , the achievable LoD is tile-dependent. We fit the coefficients of this logarithmic mapping from rate to LoD, and model the tile utility as a function of the angular resolution to replicate the empirical subjective utility-(rate, distance) curve in [37], which makes our utility model more convincing. Also, we adopt KKT to solve the continuous version of the rate allocation problem then round the rate to its discrete version. We show through simulation experiments that our method outperforms RUMA.

C. Experimental Results

We run simulations with real users' FoV traces [44] over four 8i videos. The height of the point cloud cube is $1.8m$ and roots of tiles are at 4th level of the whole octree. Each tile subtree has 6 different levels of detail. The sliding window size is $I = 20s$, and it moves forward every one second.

Table I and II display mean and variance of different metrics in different scenarios. When both the bandwidth and the FoV oracles are available (Scenario A), non-progressive streaming is comparable with progressive streaming. But in the realistic setting with network bandwidth estimation errors and FoV prediction errors (Scenario B), our proposed progressive streaming solution with either constant or exponentially decreasing frame weights can deliver much higher quality in most cases, measured using both the *quality per degree* and the *delivered angular resolution* or the number of points per viewing degree, averaged over all FoV tiles.

Test Case	Non-Progressive	Equal-Split	RUMA	Progressive KKT	
				Constant	Exp
A	18.9, 3.0	17.3, 1.6	19.5, 1.7	19.5, 1.6	N/A
B	6.1, 6.0	15.0, 2.0	15.9, 2.5	15.4, 1.8	18.3, 1.9

TABLE I: Average Frame-Angular-Resolution within the actual FoV.

Test Case	Non-Progressive	Equal-Split	RUMA	Progressive KKT	
				Constant	Exp
A	5.45, 0.42	5.34, 0.39	5.49, 0.39	5.50, 0.38	N/A
B	2.50, 1.53	5.15, 0.44	4.46, 0.63	5.16, 0.39	5.42, 0.41

TABLE II: Average Per-Degree Frame Quality

Test Case	Non-Progressive	Equal-Split	Progressive KKT	
			Constant	Exp
B	13.49 KB	6.34 KB	11.78 KB	5.19 KB

TABLE III: Average Per-frame Wasted Bandwidth: bandwidth used to download tiles that are not in the user's actual FoV.

We now analyze the results in more details. In Section V-C1, we show results for each of the four 8i videos, while the rest of the sections only present the detailed results for *Long Dress* because all the other videos have similar trends.

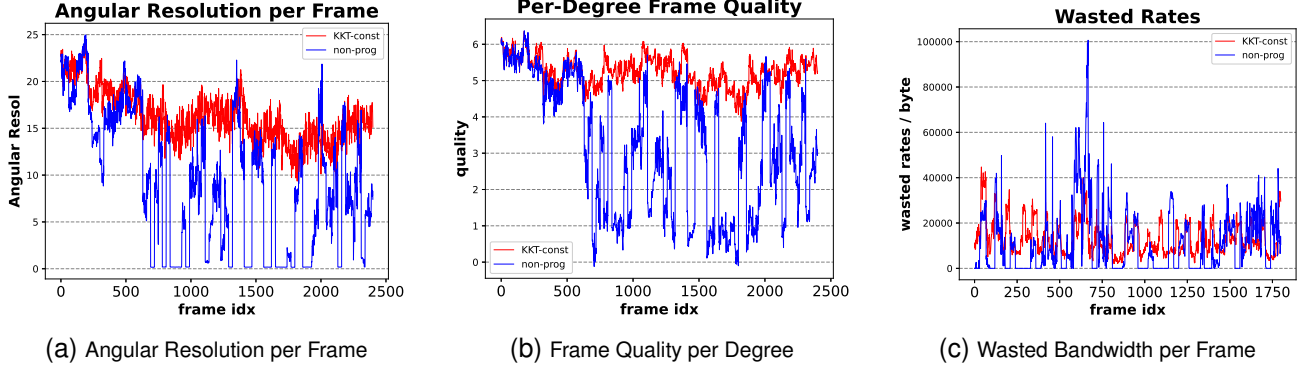


Fig. 5: Compare KKT-const and non-progressive

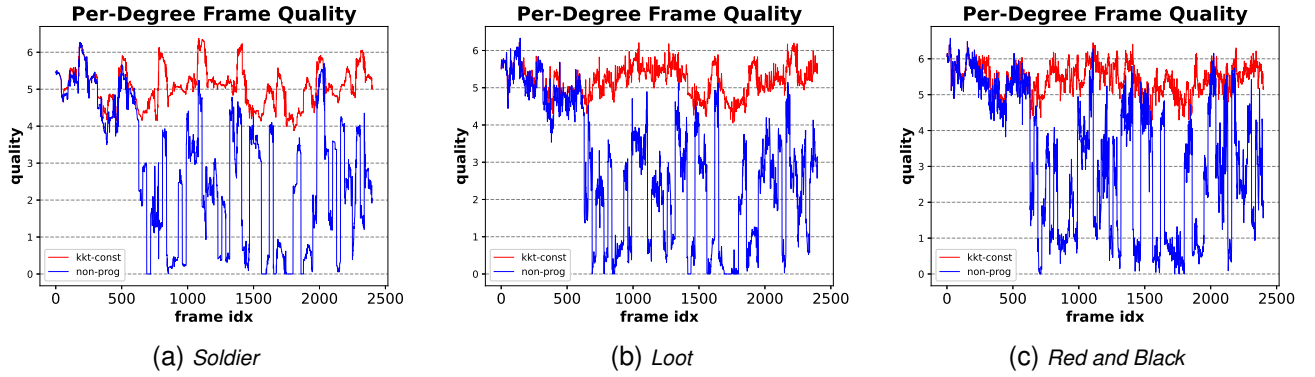


Fig. 6: Compare KKT-const and non-progressive for other videos.

1) KKT-const V.S. non-progressive:

Quality Supremacy: Only the tiles in the user’s actual FoV are counted into the final quality using Equation (2). From Fig. 5a and Fig. 5b as well as Fig. 6, we observe that except for the first 600 frames where the FoV prediction accuracy for both algorithms is accurate, KKT-const, which uses constant weights for all frames in KKT calculation, dominates non-progressive baseline in terms of both angular resolution and per-degree quality by a large gap on average. The reason is that the non-progressive baseline predicts FoV for every frame 20 seconds ahead and download the tiles only once based on the predicted FoV, which is absolutely not accurate due to the large prediction interval. Therefore, several frames have almost zero angular resolution and pretty low per-degree quality in this case. In contrast, by progressive downloading, KKT-const predicts FoV and improves the tiles’ rates for every frame over 20 rounds, with the prediction accuracy becomes more and more accurate over time.

Smoothness: The large quality variation suffered by non-progressive baseline is also due to the bandwidth variations. At each downloading round of non-progressive baseline, we allocate all the predicted available bandwidth to just one segment consisting of 30 frames that are about to enter the end of buffer. In contrast, at each downloading round of KKT-const, it updates all the frames in the buffer simultaneously based on the optimization algorithm, which smooths the resulting frame

quality evolution dramatically.

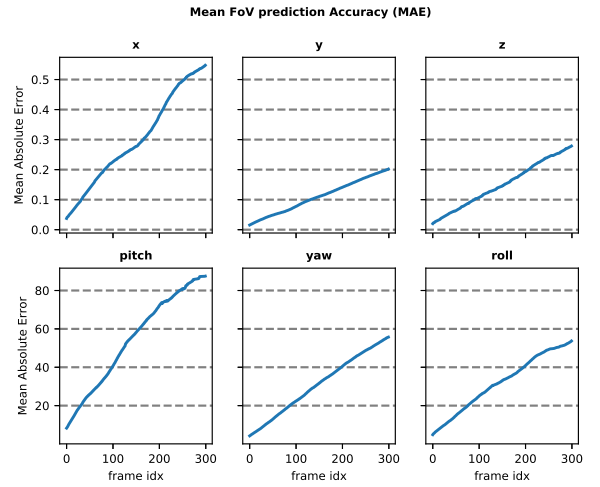


Fig. 7: Mean FoV Prediction Accuracy.

Bandwidth Consumption: At each downloading time of KKT-const, for the frames farther away from playing, e.g., 20s ahead, since the FoV prediction is not so accurate we just download a base layer for the tiles within the predicted FoV, which doesn’t waste too much bandwidth; while for the frames closer to user playback time, we patch the tiles within the more accurately predicted FoV by downloading additional enhance-

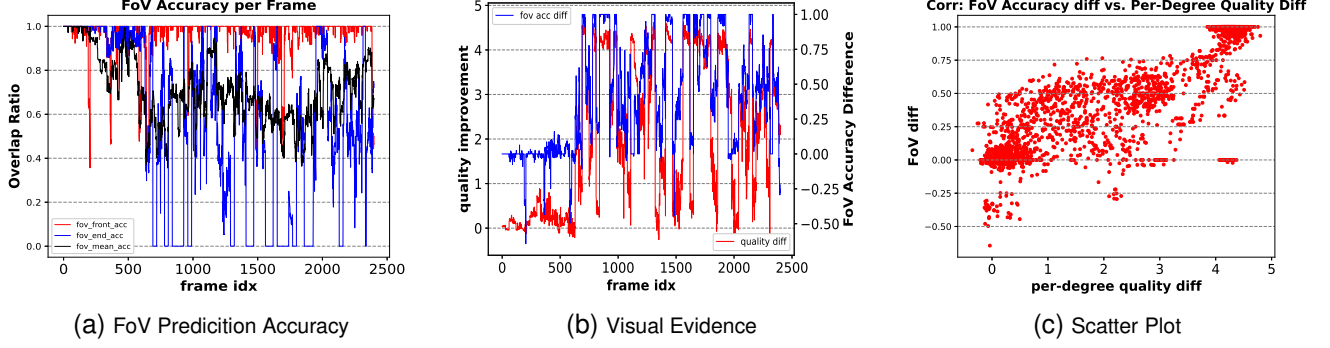


Fig. 8: Correlation between FoV Prediction Accuracy and Quality Improvement: (a) Overlap ratio between predicted and true FoV; (b) Visual evidence of the correlation; (c) Quality improvement vs. FoV prediction accuracy difference at head and tail of buffer

ment layers. However, non-progressive baseline allocates all the bandwidth to just one segment based on inaccurate FoV prediction. Therefore, in both Table III and Fig. 5c we observe that KKT-const helps save a lot of bandwidth over all the frames. The bandwidth wastage savings would be significant for long PCVs.

Correlation between Quality Improvement and FoV prediction Accuracy: To verify the motivation of progressive streaming, we zoom in to see the correlation between the quality improvements of progressive streaming and the FoV prediction accuracy. The FoV prediction accuracy in terms of Mean Absolute Error (MAE) with respect to future window sizes (at most 300 frames ahead) for 6 DoF is shown in Fig. 7. In the progressive downloading process, each frame's FoV is predicted for 20 times in a 600-frame update window. In Fig. 8a, we show the FoV prediction accuracy in terms of tile overlap ratio with ground-truth user Fov for each frame, where a larger overlap ratio means a more accurate prediction. The blue curve is the first-time prediction when the frame is just download into the buffer and far away from playback time; the red curve is the last-time prediction when the frame is closest to playback time; and black curve is the average accuracy over 20 predictions. The difference between red and blue curves in Fig. 8a represents the FoV prediction accuracy difference between the front and end position in the buffer. We also calculate the quality improvement between KKT-const and non-progressive baseline. When we put the two *difference* curves together in Fig. 8b, we find an obvious correlation between the two: if the FoV prediction at the front of the buffer (closer to user playback time) is *much better* than that at the end of buffer (way ahead of user playback time), the quality improvement of progressive-const against the non-progressive is much larger. The pattern is more obvious in the scatter-plot in Fig. 8c. The correlation coefficient is $\rho = 0.83$.

2) **KKT-exp V.S. KKT-const:** We further explore the design space of setting frame weights $\{w_i\}$ in Equation (4a). The frame weights depend on the confidence about the accuracy of FoV prediction for each frame. Therefore, intuitively, it should decrease as the prediction interval increases. We tried several different weight settings, including linear decreasing, history FoV prediction accuracy based assignment, and exponentially

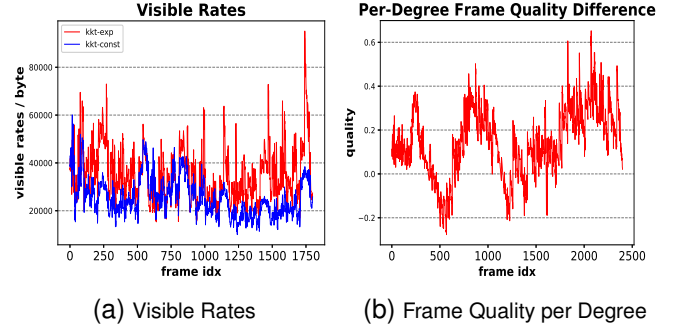


Fig. 9: KKT-exp v.s. KKT-const: (a) Visible Rate per Frame; (b) Per-degree Frame Quality Improvement.

decreasing in terms of prediction interval. We found the exponentially decreasing frame weights performs the best, as shown in Table I, II and III, as well as in Fig. 9a and 9b KKT-exp further boosts the per-degree frame quality on top of KKT-const without increasing too much quality variations. From Fig. 9a and Table III we see a large amount of bandwidth is further saved by KKT-exp.

In Fig. 9a, we can see for some frames the visible rates (i.e. the bits used inside the actual FoV) is more than doubled. That is because the long-term FoV prediction accuracy is low, and downloading tiles outside the actual FoV wastes a lot of bandwidth. We randomly pick some of these frames as an example to zoom in the improvements of tile quality in different scenarios. We show the improvement distribution over visible tiles in different network conditions, also with different FoV traces that have different distances between the user and the object, since those are two important factors affecting the final viewing quality.

Fig. 10a, 10b and 10c show the CDF of tile rate, resolution and quality improvement respectively under different network conditions and user-object distances. Resolution is the number of points per degree along one dimension in every tile. When bandwidth is high (11.5Mbps) and distance is normal (1.27m) (red curves), the average visible frame rate of KKT-const is 33 KB, KKT-exp is 86 KB, 2.6x times of KKT-const. On average,

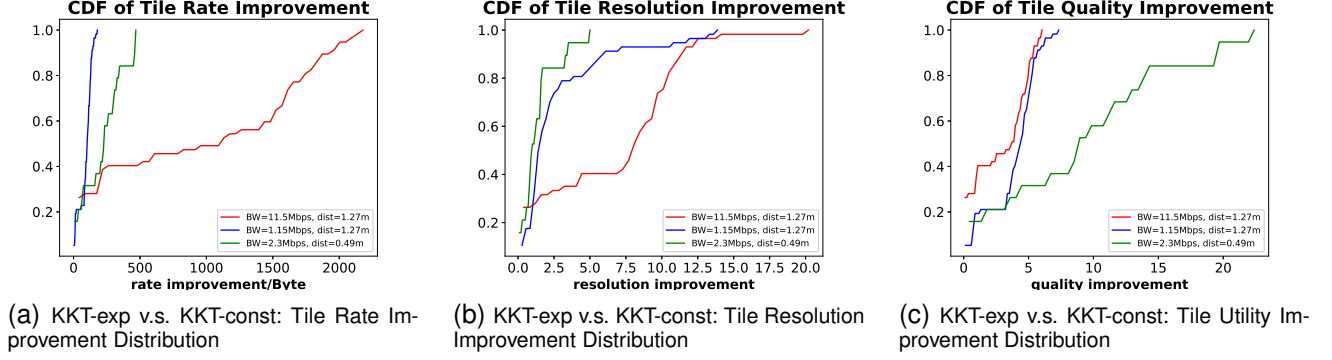


Fig. 10: KKT-exp vs KKT-const: different network conditions and user-object distances.

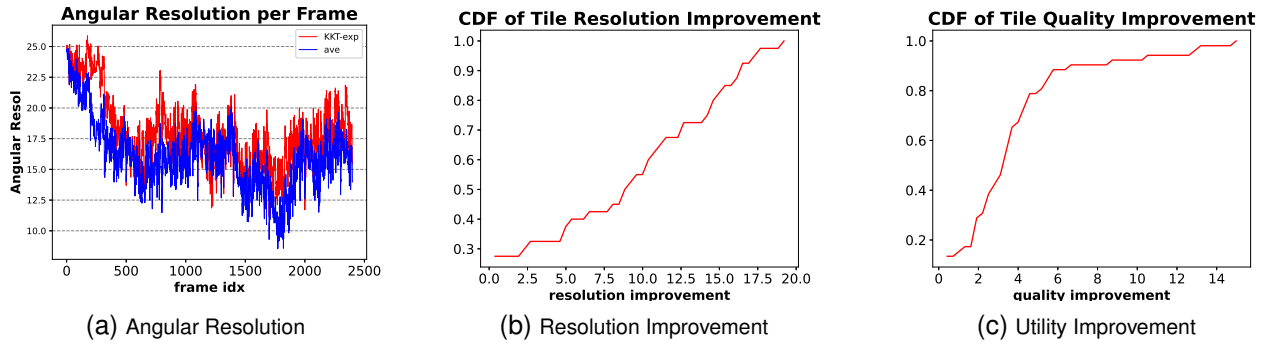


Fig. 11: KKT-exp vs Equal Allocation.

the resolution of *KKT-const* is 13 pts / degree, while *KKT-exp* is 19 pts / deg, improved by 46%. Also, the average tile quality for *KKT-const* is 28, while *KKT-exp* is 31, improved by 10.7%. Although the tiles rate difference is pretty large in this case (red curve) in Fig. 10a, the resolution difference may not be that large because some tiles have higher compression efficiency than others, or they have fewer points.

When bandwidth is small (1.15Mbps) and distance is normal (1.27m) (blue curves), the average visible frame rate of *KKT-const* is 2979 Bytes, *KKT-exp* is 8155 Bytes, 2.7x times of *KKT-const*. The average resolution in this case is 3.6 for *KKT-const* and 6.3 for *KKT-exp*. Also, the average tile quality for *KKT-const* is 19, while *KKT-exp* is 23, improved by 21.1%. Compared to the previous scenario where bandwidth is ten times larger, the tile quality now appears more sensitive to the tile rate. Therefore, although the tile rate improvement ratio is not as large as the previous scenario when bandwidth is high, the tile quality improvement ratio is similar.

We further demonstrate that tile quality is more sensitive to user-object distance change. We keep the bandwidth at a medium level (2.30Mbps), while selecting a FoV trace for which the average user-object distance is only 0.49m. Now the average frame rate improvement is 2.1 times larger. The resolution improvement is even smaller: 3.6 for *KKT-const* and 4.9 for *KKT-exp*. The absolute difference is only less than 2 pts / degree. However, the mean tile quality improvement is the largest among all scenarios as observed from the green

curve in Fig. 10c, for which the absolute improvement of *KKT-exp* compared to *KKT-const* is 9.2. This result demonstrates that the tile quality is most sensitive to tile rate when user-object distance is small. Therefore, *KKT-exp* has the greatest improvement compared to *KKT-const* when the user watches the point cloud object very closely.

3) KKT-exp V.S. Equal Allocation: To demonstrate the superiority of KKT-based tile rate allocation for PCV streaming, we design an equal allocation baseline, where the predicted available bandwidth is equally split over all the tiles within the predicted FoV of every frame. We show the frame angular resolution comparison to the equal allocation baseline in Fig. 11a, and resolution improvement CDF distribution in Fig 11b, where KKT-exp reaches 25pts/° against 17pts/° of Equal allocation. Additionally, we show mean tile quality improvement CDF in Fig. 11c.

4) KKT-exp V.S. RUMA: We now compare KKT-exp with the state-of-the-art rate allocation algorithm RUMA [36]. In Fig. 12a, we see the per-degree frame quality evolution over time. The mean per-degree quality of KKT-exp is 5.42 against 4.46 of RUMA, an improvement by 22% on average.

In Fig. 12b, we zoom in some frames whose quality improvement is larger than the others. We can see that due to the greediness of RUMA, even if some tiles have achieved the highest quality, it fails to optimize the rate allocation that should consider all the tiles of interests. Also, the intermediate steps of RUMA estimate the marginal tile utility by finite

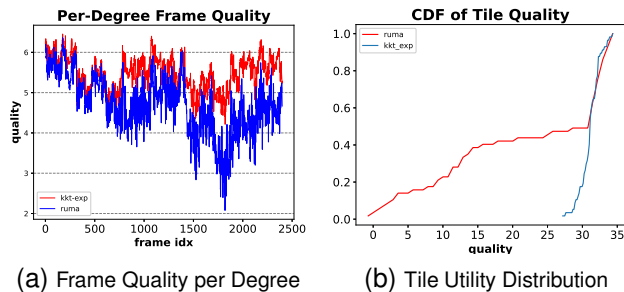


Fig. 12: KKT-exp v.s. RUMA

difference, which is not accurate enough to ensure an optimal solution. Instead, we first use KKT to solve the continuous rate allocation problem, which guarantees the optimality because we use the true marginal utility in the calculation. We then round the solution to each tile's discrete rate version.

VI. CONCLUSION

As volumetric video is on the rise, we explore the design space of point cloud video streaming which is challenging due to its high communication and computation requirements. By relying on the inherent scalability of octree-based point cloud coding, we proposed a novel *sliding-window based progressive streaming framework* to gradually refine the spatial resolution of each tile as its playback time approaches and FoV prediction accuracy improves. In this way, we managed to balance needs of long streaming buffer for absorbing bandwidth variations and short streaming buffer for accurate FoV prediction. We developed an analytically optimal algorithm based on the Karush–Kuhn–Tucker (KKT) conditions to solve the tile rate allocation problem. We also proposed a novel tile rate-utility model that explicitly considers the viewing distance to better reflect the true user QoE. In the future, we will not only consider maximizing the total tile utility, but also controlling the quality variations between consecutive frames, which leads to a more complicated non-concave objective function, and introduces stronger coupling between rate allocations on adjacent frames. We will apply nonlinear optimal control techniques, e.g. iterative Linear Quadratic Regulator (iLQR), to solve the optimal rate allocation problem.

REFERENCES

- [1] E. Cuervo, K. Chintalapudi, and M. Kotaru, "Creating the perfect illusion: What will it take to create life-like virtual reality headsets?" in *Proceedings of the 19th International Workshop on Mobile Computing Systems & Applications*, 2018, pp. 7–12.
- [2] Z. Tu, T. Zong, X. Xi, L. Ai, Y. Jin, X. Zeng, and Y. Fan, "Content adaptive tiling method based on user access preference for streaming panoramic video," in *2018 IEEE International Conference on Consumer Electronics (ICCE)*. IEEE, 2018, pp. 1–4.
- [3] Y. Zhou, L. Tian, C. Zhu, X. Jin, and Y. Sun, "Video coding optimization for virtual reality 360-degree source," *IEEE Journal of Selected Topics in Signal Processing*, vol. 14, no. 1, pp. 118–129, 2020.
- [4] M. Budagavi, J. Furton, G. Jin, A. Saxena, J. Wilkinson, and A. Dickerson, "360 degrees video coding using region adaptive smoothing," in *2015 IEEE International Conference on Image Processing (ICIP)*, 2015, pp. 750–754.
- [5] J. Zhou, N. Li, Y. Liu, S. Yao, and S. Chen, "Exploring spherical autoencoder for spherical video content processing," in *Proceedings of the 30th ACM International Conference on Multimedia*, 2022, pp. 3115–3123.
- [6] L. Hsiao, B. Krajancich, P. Levis, G. Wetzstein, and K. Winstein, "Towards retina-quality vr video streaming: 15ms could save you 80% of your bandwidth," *ACM SIGCOMM Computer Communication Review*, vol. 52, no. 1, pp. 10–19, 2022.
- [7] T. Zong, Z. Tu, L. Ai, X. Xi, Y. Jin, X. Zeng, and Y. Fan, "Panoramic video delivery based on laplace compensation and sphere-markov probability model," in *2018 IEEE International Conference on Consumer Electronics (ICCE)*. IEEE, 2018, pp. 1–4.
- [8] S. Afzal, J. Chen, and K. Ramakrishnan, "Characterization of 360-degree videos," in *Proceedings of the Workshop on Virtual Reality and Augmented Reality Network*, 2017, pp. 1–6.
- [9] M. Zink, R. Sitaraman, and K. Nahrstedt, "Scalable 360 video stream delivery: Challenges, solutions, and opportunities," *Proceedings of the IEEE*, vol. 107, no. 4, pp. 639–650, 2019.
- [10] Y. Guan, C. Zheng, X. Zhang, Z. Guo, and J. Jiang, "Pano: Optimizing 360 video streaming with a better understanding of quality perception," in *Proceedings of the ACM Special Interest Group on Data Communication*, 2019, pp. 394–407.
- [11] J. He, M. A. Qureshi, L. Qiu, J. Li, F. Li, and L. Han, "Rubiks: Practical 360-degree streaming for smartphones," in *Proceedings of the 16th Annual International Conference on Mobile Systems, Applications, and Services*, 2018, pp. 482–494.
- [12] M. Palash, V. Popescu, A. Sheoran, and S. Fahmy, "Robust 360° video streaming via non-linear sampling," in *IEEE INFOCOM 2021 - IEEE Conference on Computer Communications*, 2021.
- [13] F. Duanmu, E. Kurdoglu, Y. Liu, and Y. Wang, "View direction and bandwidth adaptive 360 degree video streaming using a two-tier system," in *2017 IEEE International Symposium on Circuits and Systems (ISCAS)*, May 2017, pp. 1–4.
- [14] F. Duanmu, E. Kurdoglu, S. A. Hosseini, Y. Liu, and Y. Wang, "Prioritized buffer control in two-tier 360 video streaming," in *Proceedings of the Workshop on Virtual Reality and Augmented Reality Network*, ser. VR/AR Network '17. New York, NY, USA: ACM, 2017, pp. 13–18. [Online]. Available: <http://doi.acm.org/10.1145/3097895.3097898>
- [15] L. Sun, F. Duanmu, Y. Liu, Y. Wang, Y. Ye, H. Shi, and D. Dai, "Multi-path multi-tier 360-degree video streaming in 5g networks," in *Proceedings of the ACM Multimedia Systems Conference*, 2018.
- [16] —, "A two-tier system for on-demand streaming of 360 degree video over dynamic networks," *IEEE Journal on Emerging and Selected Topics in Circuits and Systems*, vol. 9, no. 1, pp. 43–57, 2019.
- [17] Y. Mao, L. Sun, Y. Liu, and Y. Wang, "Low-latency fov-adaptive coding and streaming for interactive 360° video streaming," in *Proceedings of the 28th ACM International Conference on Multimedia*, 2020, pp. 3696–3704.
- [18] L. Sun, Y. Mao, T. Zong, Y. Liu, and Y. Wang, "Flocking-based live streaming of 360-degree video," in *Proceedings of the 11th ACM Multimedia Systems Conference*, 2020, pp. 26–37.
- [19] —, "Live 360 Degree Video Delivery based on User Collaboration in a Streaming Flock," *IEEE Transactions on Multimedia*, February 2022.
- [20] N. Jiang, Y. Liu, T. Guo, W. Xu, V. Swaminathan, L. Xu, and S. Wei, "Qurate: Power-efficient mobile immersive video streaming," in *Proceedings of the 11th ACM Multimedia Systems Conference*, 2020, pp. 99–111.
- [21] J. Chakareski, X. Corbillon, G. Simon, and V. Swaminathan, "User navigation modeling, rate-distortion analysis, and end-to-end optimization for viewport-driven 360 degree video streaming," *IEEE Transactions on Multimedia*, pp. 1–16, 2022.
- [22] S. Wang, S. Yang, H. Li, X. Zhang, C. Zhou, C. Xu, F. Qian, N. Wang, and Z. Xu, "Salientvr: saliency-driven mobile 360-degree video streaming with gaze information," in *Proceedings of the 28th Annual International Conference on Mobile Computing And Networking*, 2022, pp. 542–555.
- [23] Y. Bao, H. Wu, T. Zhang, A. A. Ramli, and X. Liu, "Shooting a moving target: Motion-prediction-based transmission for 360-degree videos," in *Big Data (Big Data)*, 2016 *IEEE International Conference on*. IEEE, 2016, pp. 1161–1170.
- [24] A. Nguyen, Z. Yan, and K. Nahrstedt, "Your attention is unique: Detecting 360-degree video saliency in head-mounted display for head movement prediction," in *MM 2018 - Proceedings of the 2018 ACM Multimedia Conference*, Oct. 2018, pp. 1190–1198.
- [25] J. Yu and Y. Liu, "Field-of-view prediction in 360-degree videos with attention-based neural encoder-decoder networks," in *Proceedings of*

- the 11th ACM Workshop on Immersive Mixed and Virtual Environment Systems, 2019, pp. 37–42.
- [26] J. Park, M. Wu, K.-Y. Lee, B. Chen, K. Nahrstedt, M. Zink, and R. Sitaraman, “Seaware: Semantic aware view prediction system for 360-degree video streaming,” in *2020 IEEE International Symposium on Multimedia (ISM)*. IEEE, 2020, pp. 57–64.
 - [27] C. Li, W. Zhang, Y. Liu, and Y. Wang, “Very long term field of view prediction for 360-degree video streaming,” in *2019 IEEE Conference on Multimedia Information Processing and Retrieval (MIPR)*. IEEE, 2019, pp. 297–302.
 - [28] J. Dai, Z. Zhang, S. Mao, and D. Liu, “A view synthesis-based 360° vr caching system over mec-enabled c-ran,” *IEEE Transactions on Circuits and Systems for Video Technology*, vol. 30, no. 10, pp. 3843–3855, 2019.
 - [29] J. Liu, G. Simon, X. Corbillion, J. Chakareski, and Q. Yang, “Delivering viewport-adaptive 360-degree videos in cache-aided mec networks,” in *2020 IEEE International Symposium on Broadband Multimedia Systems and Broadcasting (BMSB)*. IEEE, 2020, pp. 1–6.
 - [30] A. Sarkar, J. Murray, M. Dasari, M. Zink, and K. Nahrstedt, “L3bou: Low latency, low bandwidth, optimized super-resolution backhaul for 360-degree video streaming,” in *2021 IEEE International Symposium on Multimedia (ISM)*. IEEE, 2021, pp. 138–147.
 - [31] C. Li, T. Ye, T. Zong, L. Sun, H. Cao, and Y. Liu, “Coffee: Cost-effective edge caching for 360 degree live video streaming,” *arXiv preprint arXiv:2312.13470*, 2023.
 - [32] R. Chen, M. Xiao, D. Yu, G. Zhang, and Y. Liu, “patchvvc: A real-time compression framework for streaming volumetric videos,” in *Proceedings of the 14th Conference on ACM Multimedia Systems*, 2023, pp. 119–129.
 - [33] S. Wang, M. Zhu, N. Li, M. Xiao, and Y. Liu, “Vqba: Visual-quality-driven bit allocation for low-latency point cloud streaming,” in *Proceedings of the 31st ACM International Conference on Multimedia*, 2023, pp. 9143–9151.
 - [34] J. Zhang, T. Chen, D. Ding, and Z. Ma, “G-pcc++: Enhanced geometry-based point cloud compression,” in *Proceedings of the 31st ACM International Conference on Multimedia*, 2023, pp. 1352–1363.
 - [35] Y. Wang, D. Zhao, H. Zhang, C. Huang, T. Gao, Z. Guo, L. Pang, and H. Ma, “Hermes: Leveraging implicit inter-frame correlation for bandwidth-efficient mobile volumetric video streaming,” in *Proceedings of the 31st ACM International Conference on Multimedia*, 2023, pp. 9185–9193.
 - [36] J. Park, P. A. Chou, and J.-N. Hwang, “Rate-utility optimized streaming of volumetric media for augmented reality,” *IEEE Journal on Emerging and Selected Topics in Circuits and Systems*, vol. 9, no. 1, pp. 149–162, 2019.
 - [37] B. Han, Y. Liu, and F. Qian, “Vivo: Visibility-aware mobile volumetric video streaming,” in *Proceedings of the 26th annual international conference on mobile computing and networking*, 2020, pp. 1–13.
 - [38] K. Lee, J. Yi, Y. Lee, S. Choi, and Y. M. Kim, “Groot: A real-time streaming system of high-fidelity volumetric videos,” in *Proceedings of the 26th Annual International Conference on Mobile Computing and Networking*, ser. MobiCom ’20. New York, NY, USA: Association for Computing Machinery, 2020. [Online]. Available: <https://doi.org/10.1145/3372224.3419214>
 - [39] A. Zhang, C. Wang, B. Han, and F. Qian, “YuZu: Neural-Enhanced Volumetric Video Streaming,” in *19th USENIX Symposium on Networked Systems Design and Implementation (NSDI 22)*, 2022, pp. 137–154.
 - [40] Y. Liu, B. Han, F. Qian, A. Narayanan, and Z.-L. Zhang, “Vues: practical mobile volumetric video streaming through multiview transcoding,” in *Proceedings of the 28th Annual International Conference on Mobile Computing and Networking*, 2022, pp. 514–527.
 - [41] L. Wang, C. Li, W. Dai, J. Zou, and H. Xiong, “Qoe-driven and tile-based adaptive streaming for point clouds,” in *ICASSP 2021-2021 IEEE International Conference on Acoustics, Speech and Signal Processing (ICASSP)*. IEEE, 2021, pp. 1930–1934.
 - [42] L. Wang, C. Li, W. Dai, S. Li, J. Zou, and H. Xiong, “Qoe-driven adaptive streaming for point clouds,” *IEEE Transactions on Multimedia*, 2022.
 - [43] S. Rossi, I. Viola, L. Toni, and P. Cesar, “Extending 3-dof metrics to model user behaviour similarity in 6-dof immersive applications,” in *Proceedings of the 14th Conference on ACM Multimedia Systems*, 2023, pp. 39–50.
 - [44] S. Subramanyam, I. Viola, A. Hanjalic, and P. Cesar, “User centered adaptive streaming of dynamic point clouds with low complexity tiling,” in *Proceedings of the 28th ACM international conference on multimedia*, 2020, pp. 3669–3677.
 - [45] J. Kammerl, N. Blodow, R. B. Rusu, S. Gedikli, M. Beetz, and E. Steinbach, “Real-time compression of point cloud streams,” in *2012 IEEE international conference on robotics and automation*. IEEE, 2012, pp. 778–785.
 - [46] Y. Shi, P. Venkatram, Y. Ding, and W. T. Ooi, “Enabling low bit-rate mpeg v-pcc-encoded volumetric video streaming with 3d sub-sampling,” in *Proceedings of the 14th Conference on ACM Multimedia Systems*, 2023, pp. 108–118.
 - [47] R. Mekuria, K. Blom, and P. Cesar, “Design, implementation, and evaluation of a point cloud codec for tele-immersive video,” *IEEE Transactions on Circuits and Systems for Video Technology*, vol. 27, no. 4, pp. 828–842, 2016.
 - [48] A. Zhang, C. Wang, B. Han, and F. Qian, “Efficient volumetric video streaming through super resolution,” in *Proceedings of the 22nd International Workshop on Mobile Computing Systems and Applications*, 2021, pp. 106–111.
 - [49] X. Sheng, L. Li, D. Liu, Z. Xiong, Z. Li, and F. Wu, “Deep-pcac: An end-to-end deep lossy compression framework for point cloud attributes,” *IEEE Transactions on Multimedia*, vol. 24, pp. 2617–2632, 2021.
 - [50] J. Wang, H. Zhu, H. Liu, and Z. Ma, “Lossy point cloud geometry compression via end-to-end learning,” *IEEE Transactions on Circuits and Systems for Video Technology*, vol. 31, no. 12, pp. 4909–4923, 2021.
 - [51] Y. Mao, Y. Hu, and Y. Wang, “Learning to predict on octree for scalable point cloud geometry coding,” in *2022 IEEE 5th International Conference on Multimedia Information Processing and Retrieval (MIPR)*. IEEE, 2022, pp. 96–102.
 - [52] Z. Liu, J. Li, X. Chen, C. Wu, S. Ishihara, and Y. Ji, “Fuzzy logic-based adaptive point cloud video streaming,” *IEEE Open Journal of the Computer Society*, vol. 1, pp. 121–130, 2020.
 - [53] J. Van Der Hooft, T. Wauters, F. De Turck, C. Timmerer, and H. Hellwagner, “Towards 6dof http adaptive streaming through point cloud compression,” in *Proceedings of the 27th ACM International Conference on Multimedia*, 2019, pp. 2405–2413.
 - [54] Y. Gao, P. Zhou, Z. Liu, B. Han, and P. Hui, “Fras: Federated reinforcement learning empowered adaptive point cloud video streaming,” *arXiv preprint arXiv:2207.07394*, 2022.
 - [55] J. Li, C. Zhang, Z. Liu, R. Hong, and H. Hu, “Optimal volumetric video streaming with hybrid saliency based tiling,” *IEEE Transactions on Multimedia*, 2022.
 - [56] J. Li, H. Wang, Z. Liu, P. Zhou, X. Chen, Q. Li, and R. Hong, “Towards optimal real-time volumetric video streaming: A rolling optimization and deep reinforcement learning based approach,” *IEEE Transactions on Circuits and Systems for Video Technology*, 2023.
 - [57] M. Rudolph, S. Schneegass, and A. Rizk, “Rabbit: Live transcoding of v-pcc point cloud streams,” in *Proceedings of the 14th Conference on ACM Multimedia Systems*, 2023, pp. 97–107.
 - [58] J. Zhang, T. Chen, D. Ding, and Z. Ma, “Yoga: Yet another geometry-based point cloud compressor,” in *Proceedings of the 31st ACM International Conference on Multimedia*, 2023, pp. 9070–9081.
 - [59] D. Graziosi, O. Nakagami, S. Kuma, A. Zaghetto, T. Suzuki, and A. Tabatabai, “An overview of ongoing point cloud compression standardization activities: Video-based (v-pcc) and geometry-based (g-pcc),” *APSIPA Transactions on Signal and Information Processing*, vol. 9, 2020.
 - [60] Google. (2017) Draco 3d data compression. [Online]. Available: <https://google.github.io/draco/>
 - [61] M. Hosseini and C. Timmerer, “Dynamic adaptive point cloud streaming,” in *Proceedings of the 23rd Packet Video Workshop*, 2018, pp. 25–30.
 - [62] J. H. Westerink and J. A. Roufs, “Subjective image quality as a function of viewing distance, resolution, and picture size,” *SMPTE journal*, vol. 98, no. 2, pp. 113–119, 1989.
 - [63] wikipedia, “visual acuity,” 2023. [Online]. Available: https://en.wikipedia.org/wiki/Visual_acuity
 - [64] E. d’Eon, B. Harrison, T. Myers, and P. A. Chou, “8i voxelized full bodies-a voxelized point cloud dataset,” *ISO/IEC JTC1/SC29 Joint WG11/WG1 (MPEG/JPEG) input document WG11M40059/WG1M74006*, vol. 7, no. 8, p. 11, 2017.
 - [65] L. Mei, R. Hu, H. Cao, Y. Liu, Z. Han, F. Li, and J. Li, “Realtime mobile bandwidth prediction using lstm neural network,” in *Passive and Active Measurement: 20th International Conference, PAM 2019, Puerto Varas, Chile, March 27–29, 2019, Proceedings 20*. Springer, 2019, pp. 34–47.